Title
Polyamide-Based Ion Exchange Membranes: Cation-Selective Transport through Water Purification Membranes

Journal
ACS Applied Polymer Materials, 6(3)

ISSN
2637-6105

Authors
Wang, Jingbo
Lim, Jeonghoon
Wang, Monong
et al.

Publication Date
2024-02-09

DOI
10.1021/acsapm.4c00001

ACS APPLIED POLYMER MATERIALS

pubs.acs.org/acsapm
Article

Polyamide-Based Ion Exchange Membranes: Cation-Selective Transport through Water Purification Membranes

Jingbo Wang, Jeonghoon Lim, Monong Wang, Baoxia Mi, Daniel J. Miller, and Bryan D. McCloskey*

Cite This: ACS Appl. Polym. Mater. 2024, 6, 2022−2030
Read Online

ABSTRACT: Ion-selective membranes are necessary components of many electrochemical systems including fuel cells, electrolyzers, redox flow batteries, and electrodialyzers. Perfluorinated sulfonated membranes (PFSMs) dominate these applications due to their excellent combination of fast ion transport, stability, and processability. However, perfluorinated cation exchange membranes (CEMs) are expensive, and their production process involves chemistry that generates toxic perfluorinated chemicals. The development of affordable, nonfluorinated membranes with a competitive combination of high ion selectivity, transport, and stability could help enable the widespread use of the technologies listed above while hastening the development of emerging electrochemical systems, including aqueous alkaline CO_2 sorbent regeneration. To this end, we pursue the use of thin-film composite polyamide (PA-TFCs) membranes—those that typically find application in reverse osmosis and nanofiltration desalination—as cation-selective exchange membranes. Given their negative surface charge under neutral-to-alkaline conditions, PA-TFCs can serve as effective CEMs in these pH regimes. We prepared a series of PA-TFCs from traditional monomers (trimesoyl chloride and piperazine) and compared their thicknesses, charge densities, water transport properties, ion transport properties, and long-term stability in a high pH environment to traditional CEMs (Nafion and FKE) and commercial nanofiltration and reverse osmosis membranes. We find that some of the best-performing PA-TFC membranes have similar resistances and Na^+ transference numbers compared to Nafion 117 in Na_2SO_4 and $NaHCO_3$-containing solutions. This proof-of-principle study suggests that further optimization of PA-TFCs could enable cost-effective ion exchange membrane alternatives to PFSMs.

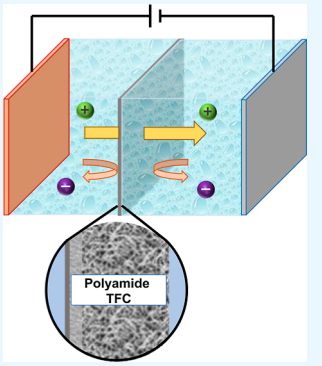

KEYWORDS: *thin-film composite membrane, polyamide, electrochemical flow system, ion transport, carbon capture, CO_2 sorbent regeneration*

1. INTRODUCTION

Perfluorinated sulfonated membranes (PFSMs) such as Nafion are typically used for the selective cation transport in electrochemical flow systems.[1−5] As current commercial PFSMs are extremely expensive and their production process involves unsustainable chemistry that generates toxic perfluorinated species, researchers have been exploring alternative approaches for improving the economic and sustainable viability of cation exchange membranes (CEMs).[1−3] In particular, new cost-effective membrane alternatives are imperative to enable emerging clean technologies, such as alkaline CO_2 sorbent regeneration for direct air CO_2 capture (DAC), redox flow batteries, and electrodialysis.

To this end, we investigate the ion transport in membranes based on the chemistry of reverse osmosis (RO) membranes. Current RO membrane costs are over an order of magnitude lower than Nafion, with long operational lifetimes (>10 years) proven in aggressive conditions (wide pH ranges, with high pressures and temperatures).[6] RO membranes reject salt in pressure-driven processes through a complex combination of dielectric exclusion and Donnan exclusion.[7−10] Our efforts focus on leveraging Donnan exclusion, which occurs when the negatively charged polyamide (PA) selective layer impedes anion transport, and due to electroneutrality, cations are also rejected. In principle, Donnan exclusion could be leveraged to promote a fast, selective cation transport through appropriately designed selective layers when driven by an electric field. RO membranes have been engineered to largely reject salt and allow a modest water transport due to their tight, highly cross-linked PA structures. We hypothesized that a highly charged, swollen (low degrees of cross-linking) PA structure will enable a fast cation transport while inhibiting anion transport via the Gibbs−Donnan effect when using an electric field driving force.

While ion transport in these PA-based thin-film composite (TFC) membranes has been extensively studied in processes for desalination applications,[11−18] only a few studies have been

Received: January 1, 2024
Revised: January 13, 2024
Accepted: January 16, 2024
Published: January 26, 2024

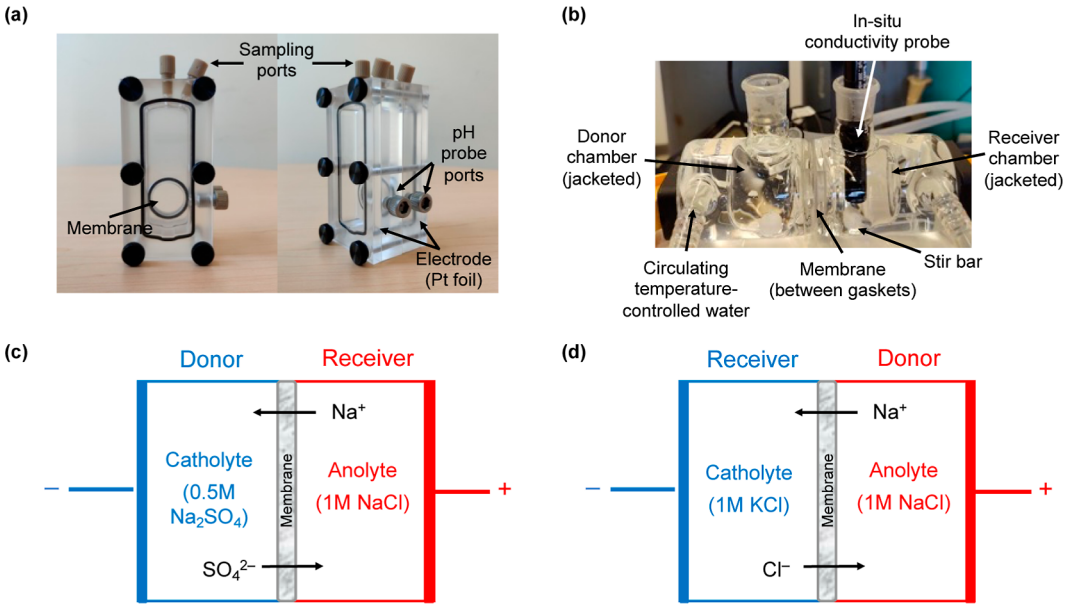

Figure 1. (a) Photo of the electrochemical cell for resistance and transference number measurements. (b) Photo of the diffusion cell used to measure the salt permeation coefficient. (c,d) Schematic diagrams of the ion transference number measurement setups that estimate the SO_4^{2-} transference number in 0.5 M Na_2SO_4 (c) or the Na^+ transference number in NaCl (d).

reported on ion transport with an applied electrical field as would be required in electrochemical flow systems.[19−26] While Bason et al.[23,27,28] developed a method to study transport of a redox ion couple in PA brackish water membranes, other studies focused on investigating system performance when implementing PA-based TFCs in electrochemical processes including electrolysis,[19] electrodialysis-based separations,[20,21,24−26] and flow batteries.[22] In particular, Shi et al.[19] examined the potential for using commercial RO membranes as proton-selective membranes for seawater electrolysis applications and reported that brackish water membranes showed acceptable performance, with low membrane resistances leading to low electrolysis overpotential. However, we are not aware of studies that focus on the cation−anion selectivity of PA membranes in contact with various electrolytes (many studies focus on "like" charged ion selectivities, either cation−cation or anion−anion) as would be necessary to understand the utility of PA composite membranes as CEMs. Nor are we aware of studies that attempt to link the PA layer thickness and the charge density to ion selectivity and membrane resistance, which would provide insight into an appropriate membrane design to achieve desirable ion transport properties for various electrochemical applications.

Building on this previous research study, the goal of this study is to redesign robust and cost-effective PA-based membranes that could be used in electrochemical flow systems in "near-neutral" (~pH 3−12) conditions, which are applicable to water purification (electrodialysis) systems, neutral pH redox flow batteries,[29,30] and buffered carbonate sorbents for direct air capture.[31] We aim to understand how the membrane's physical properties (e.g., PA layer thickness and charge density) impact membrane resistance and, importantly for CEMs, cation-to-anion selectivity as defined by the transference number (described below). We synthesize a series of PA-TFC membranes using the common trimesoyl chloride (TMC) and piperazine (PIP) monomers to systematically change the PA layer thickness and the charge density. We compare transport through these membranes to commercially available RO and nanofiltration (NF) membranes as well as more traditional PFSMs (Nafion 117 and FKE). We show that certain PA-TFC membranes have Na^+ ion selectivities and resistances comparable to Nafion 117 and FKE, highlighting their potential as affordable CEMs in emerging electrochemical systems.

2. MATERIALS AND METHODS

2.1. Membranes. Commercial perfluorinated CEMs, including Nafion 117 (Chemours, Wilmington, DE) and FKE (Fumasep, Germany), were used to benchmark the membrane performance. Two commercial PA-based membranes were chosen for comparison: a brackish water RO membrane (XLE, DuPont Water Solutions, MN) and a high-flux NF membrane (NFG, Synder Filtration, CA). A series of PA-TFC membranes were fabricated in-house via interfacial polymerization[32,33] between TMC (0.15 wt % in Isopar G) and PIP (0.2−2.0 wt % in deionized water, DI) atop a porous poly(ether sulfone) (PES) support (LX, Synder Filtration, CA) using 1 min of polymerization time as described similarly elsewhere[34] (Section S1 in Supporting Information). These hand-cast membranes are referred to as M-2.0, M-1.0, M-0.5, and M-0.2 membranes throughout this study, where the numbers reflect PIP weight percentage in the aqueous phase polymerization solution used in the synthesis process. All of the membranes were stored in DI water prior to their characterization.

2.2. Membrane Thickness Measurements. The PA layer thicknesses were measured using two separate methods: quartz crystal microbalancing (QCM) and ellipsometry. For the QCM method, the PA layer was isolated onto a QCM sensor using a procedure described previously (Section S7 in Supporting Information).[35] The PA layer mass (m_{PA}, ng cm^{-2}) was measured using QCM, and the PA thickness (δ, nm) was then calculated as

$$\delta = \frac{m_{PA}}{\rho_{PA}} \quad (1)$$

where ρ_{PA} = 1.24 g cm^{-3} corresponds to the typical mass density of the PA layer.[36]

Ellipsometry was also used to quantify all of the PA layer thicknesses. Here, the PA layer was isolated onto a silicon wafer using the method of Lin et al. (Section S7 in Supporting Information).[36] Ellipsometry data were obtained with an ellipsometer (FS-1 Multiwavelength, Film Sense, Lincoln, NE) measuring the phase

https://doi.org/10.1021/acsapm.4c00001
ACS Appl. Polym. Mater. 2024, 6, 2022−2030

change and the amplitude ratio between the parallel and perpendicular light polarizations reflected from the sample as a function of light wavelength and incidence angle. This information is then used for fitting a complete electromagnetic model of the sample, with the refractive index and the thickness of the sample as adjustable parameters. The Cauchy dispersion equation was used to determine the optical properties of the active PA layers and calculate the layer thickness. The sample was modeled as a two-layer composite, with the bottom layer being silicon with a native oxide film and the top layer being the thin PA layer. To accurately calculate the PA layer thickness, a measurement was first taken for the base Si substrate used for the sample preparation to calculate its optical constant. After another measurement was taken for the PA-coated Si sample, a second layer was added to the model to determine the optical constants and the thickness of the PA layer while keeping the predetermined constants for Si fixed. The adjustable parameters in this study were the refractive index and the PA layer thickness, and their values were changed to best fit the model. The calculated refractive index was compared with a database in the literature and on the web[37] to avoid over- or underfitting. Three samples were analyzed for each membrane, with three locations (0.3 cm^2 each location) analyzed for each sample.

2.3. Resistance Measurements. The ionic resistance of the different membranes was measured using electrochemical impedance spectroscopy (EIS) at room temperature, using a method outlined by Kamcev et al.[38] Prior to resistance measurements, all membranes were equilibrated in aqueous Na_2SO_4 solutions at concentrations ranging from 0.1 to 1.5 M. We use Na_2SO_4 here as a potential cost-effective supporting electrolyte for any electrochemical flow system but also report on the transport of other salts later. The equilibration procedure consisted of soaking the membranes in Na_2SO_4 solutions for at least 24 h, where the solutions were periodically replaced to ensure a constant salt concentration in the equilibrating solution. The resistance measurements were performed using the EIS technique with a SP-300 Potentiostat (Biologic, France). The configuration employed a two-electrode setup, where the counter and working electrodes were platinum foils of area 25 cm^2 (0.025 mm thick, 99.99% metal basis, Thermo Scientific, Waltham, MA). The measurements were performed over a frequency range of 0.01−200 kHz, which was sufficient to extract the ohmic resistance between the two platinum electrodes. A custom-made acrylic cell (College of Chemistry Machine Shop, Berkeley, CA) was used for this measurement (Figure 1a), providing a planar configuration between the electrodes with a well-mixed (via stir bar) electrolyte gap on each side of the membrane. Each 25 mL chamber had two 5/16″ sampling ports at the top, one 1/4″ ports for a pH probe on the side, and a vertical face with a 1″ orifice where the membrane sits and separates each chamber. The distance between the membrane and each electrode was 20 mm. In each experiment, the fully hydrated membrane was sandwiched between the two chambers. The ohmic resistance of the electrochemical cell, which includes the electrolyte solution and membrane (R_{m+s}, Ω), was taken as the value of the real impedance when the imaginary impedance was zero (i.e., when the data on a Nyquist plot crossed the real axis). Representative Nyquist plots for experiments performed using the difference method are presented in Figure S1 in Supporting Information. After the measurement, the cell was disassembled and then reassembled without the membrane, and the measurement was repeated to obtain the resistance of the solution (R_s, Ω). The membrane resistance (R_m, Ω) was determined as

$$R_m = R_{m+s} - R_s \tag{2}$$

2.4. Membrane Charge Density Measurements. The concentration of a fixed negative charge in the active layer of the TFC membranes at pH = 11.0, 9.5, 7.5, and 5.5 was measured using a QCM (Nanoscience Instruments, AZ) method as described in detail in previous works.[35,39,40] In brief, a QCM sensor (Nanoscience Instruments, AZ) was coated with a PA layer isolated from a TFC membrane using a procedure similar to that used in the ellipsometry thickness measurements described above. As membranes were stored in DI water after fabrication, membranes are in their protonated form prior to charge density measurements. The negative fixed charges were then saturated with cesium ions (Cs^+) by exposing the coated sensors to a 0.001 M cesium chloride (CsCl) solution at pH 11.0, 9.5, 7.5, and 5.5. The corresponding mass of Cs^+ (m_{Cs}, ng cm^{-2}) neutralizing the fixed charges in each sensor was measured with QCM. Given that Cs^+ has on average less than one water molecule of hydration,[41] and there is a 1:1 correspondence between carboxylate groups and Cs^+ ions, the molar concentration of fixed charges (C_{charge}, mequiv g^{-1}) was calculated as

$$C_{charge} = \frac{m_{Cs}}{MW_{Cs} \cdot m_{PA}} \times 1000 \tag{3}$$

where MW_{Cs} = 132.91 g·mol^{-1} is the molecular weight of cesium and m_{PA} (ng cm^{-2}) is the dry mass of the PA layer.

2.5. Solute Permeation Measurement. Salt permeation experiments were carried out using a standard diffusion cell (Figure 1b; Adams and Chittenden Scientific Glassware, Berkeley, CA). Each 40 mL half-cell had a 3/8 in. sampling port at the top and a vertical ground glass face with a 15 mm orifice. The fully hydrated membrane was sandwiched between two silicone gaskets with a 15 mm orifice in their centers, and this sandwich was clamped between the two-half cells. The half cells were jacketed, and water was circulated through the jackets to maintain the solution temperature at 25 °C throughout each experiment. One of the two identical half cells (the receiver chamber) was filled with 38 mL of ultrapure water, and the other half cell (the donor chamber) was filled with 38 mL of 1 M NaCl or 1 M Na_2SO_4 solution. A conductivity probe (Orion DuraProbeTM 4-Cell conductivity probe, Thermo Scientific, MA) was inserted into the receiver chamber, ensuring that the probe tip was fully immersed. The conductivity of the receiver chamber was recorded by a conductivity meter (Orion Star A215 pH/Conductivity Benchtop Multiparameter Meter, Thermo Scientific, MA) at 10 s intervals for 30 min. The permeation coefficient of a solute (B, m/s) can be obtained by[42−44]

$$B = -\ln\left(1 - 2\frac{C_R}{C_{D,0}}\right)\cdot\frac{V}{2At} \tag{4}$$

where C_R (M) is the time-dependent solute concentration in the receiver chamber, $C_{D,0}$ (M) is the solute concentration in the donor chamber at the beginning of the experiment, V (3.8×10^{-4} m^3) is the volume of solution in the donor chamber (equal volume of solution in the receiver chamber in all experiments), A (1.33×10^{-4} m^2) is the effective membrane area, and t (s) is the experimental duration.

2.6. Ion Transference Number Measurement. The transference number of an ion is the fraction of current passed through an electrolyte that is carried by that ion, effectively making it a measure of ion transport selectivity in electrolytes and membranes. To measure the Na^+ transference number in our membranes, the custom-made acrylic electrochemical cell, described in the Membrane Resistance section, was used (Figure 1a). A Biologic SP-300 Potentiostat was used to apply a constant current of 100 mA between the electrodes, corresponding to a current density of 19.7 mA cm^{-2}. The pH of each chamber was monitored using a portable pH meter (Orion Star A220, Thermo Scientific, MA) with a micro pH probe (Orion PerpHecT ROSS, Thermo Scientific, MA). We use the method developed by Vardner et al.[45,46] in symmetric and asymmetric electrolyte systems for these measurements. For each piece of membrane tested, the chambers were filled with 24 mL of fresh solution, either 0.5 M Na_2SO_4 (catholyte) and 1 M NaCl (anolyte) or 1 M KCl (catholyte) and 1 M NaCl (anolyte). By passing a large current through the membrane/electrolyte in a cell with an appropriate electrolyte orientation, the ion flux due to migration (electric field-driven transport) far outweighs any ion flux due to diffusion (concentration gradient-driven flux). By monitoring the concentration of ions in each chamber as a function of total electric capacity (mA h) passed through the membrane, we are able to then back calculate the total current carried by each ion and therefore quantify the ion transference number. As an example, Figure 1d shows the configuration in which NaCl and KCl are placed in chambers on either side of the membrane. By placing NaCl in the anolyte chamber and passing the

https://doi.org/10.1021/acsapm.4c00001
ACS Appl. Polym. Mater. 2024, 6, 2022−2030

Table 1. Summary of the PA Layer Thickness[a] Measured with Two Methods and Commercial CEM Thickness[b]

membrane	NFG	XLE	M-2.0	M-1.0	M-0.5	M-0.2	Nafion	FKE
thickness by ellipsometry (nm)	14 ± 2	135 ± 4	59 ± 6	46 ± 6	20 ± 2	12 ± 1	175 μm	50 μm
thickness by QCM (nm)	21 ± 4	127 ± 5	62 ± 16	50 ± 1	25 ± 1	18 ± 2		

[a]The thickness reported here for PA membranes only reflects the thickness of the PA layer without the support layers, not the thickness of the TFC. Reported values and uncertainties correspond to the average and standard deviation of triplicate samples. [b]The thickness of commercial PFSMs was obtained from manufacture information sheets.

current between the electrodes, we expect Na^+ to migrate through the membrane to the catholyte chamber and Cl^- to migrate in the opposite direction from the catholyte chamber to the anolyte chamber. By placing KCl in the catholyte chamber, we can accurately quantify small Na^+ concentration differences in this chamber, allowing the accurate quantification of its flux through the membrane. In the limit of high current densities, we expect comparatively negligible K^+ diffusive or migrational flux in the opposite direction, thereby making Na^+ and Cl^- the ions predominantly carrying current through the membrane and enabling calculation of the Na^+ transference number, as outlined below. Given that Na^+ and Cl^- carry the large majority of current through the membrane, this procedure provides a good estimation of the transference number expected in a NaCl solution, even though the catholyte is KCl. A similar configuration to estimate the transference number of a Na_2SO_4 solution is shown in Figure 1c, where the same principle is used and we monitor the concentration buildup of the SO_4^{2-} anion. A total constant current of 100 mA (19.7 mA cm^{-2}) was applied between the electrodes for 25 min, thereby forming OH^- via hydrogen evolution at the cathode and H^+ via oxygen evolution at the anode. Ions will migrate across the membrane to ensure that electroneutrality in each chamber is maintained. Each electrolyte chamber was well-stirred. A 0.05 mL sample was taken every 5 min from the receiving chamber (the catholyte chamber for KCl|NaCl cells, the anolyte chamber for Na_2SO_4|NaCl cells) for Na^+ and SO_4^{2-} ion concentration analyses, respectively, until measurement completion. The 25 min measurements were used to ensure that the OH^- and H^+ concentrations in the catholyte and anolyte, respectively, never increased to above 0.01 M (or 100 times smaller than the ions of interest), ensuring that their contributions to the measured current was negligible. Linear concentration increases of Na^+ or SO_4^{2-} in the receiver chambers over the course of the measurements further confirm that H^+ and OH^- do not substantially contribute to the ion transport (the Na^+ and SO_4^{2-} concentrations would start to "level off" as the concentrations of H^+ and OH^- increase during the measurements; see Figure S5). Ion concentrations were measured using an inductively coupled plasma with an optical emission system (ICP-OES, PerkinElmer, MA). The ionic flux (J_j, mol cm^{-2} s^{-1}) was determined from the concentration measurements according to Fick's first law

$$J_j = \frac{d(V \cdot C_j)}{A \cdot dt} \quad (5)$$

where C_j (M) is the time-dependent ion "j" concentration in the receiver cell, V (L) is the electrolyte volume, A (5.065 cm^2) is the effective membrane area, and t (s) is the time. As the current density across the membrane is carried by the mobile ions within the electrolyte, the total current density (i, A cm^{-2}) can be related to the flux of ions by the following expression

$$i = F \sum_j z_j J_j \quad (6)$$

where z_j (unitless) is the charge of species j and F (A s mol^{-1}) is Faraday's constant. Then, the transference number of an ion (t_j, unitless) can be calculated using

$$t_j = \frac{F z_j J_j}{i} \quad (7)$$

3. RESULTS AND DISCUSSION

3.1. Membrane Thickness. The membrane thickness results are summarized in Table 1. The thickness measured with both the QCM and ellipsometry was similar for each individual membrane, with less than 7.5 nm difference between the two measurement methods across all samples. As expected, XLE has the thickest PA layer due to the different fabrication procedures used to produce commercial RO membranes. All fabricated TFCs had much thinner PA layers, similar in magnitude to the commercial NF membrane, NFG. Among the fabricated TFCs, the PA thickness decreased from 59 ± 6 nm to 12 ± 1 nm as the amine monomer concentration decreased from 2.0 to 0.2%. Our results suggest that the correlation between PIP concentration and the PA layer thickness could be used in the future as a guide to fabricate PA layers with the desired thickness.

3.2. Membrane Resistance. The membrane resistances in different concentrations of the Na_2SO_4 electrolytes are reported in Figure 2. We use Na_2SO_4 as the electrolyte given

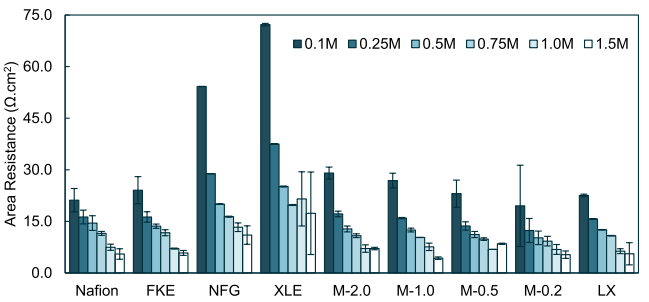

Figure 2. Membrane resistance measured with EIS, including two commercial CEMs (Nafion, FKE), two commercial TFCs (NFG, XLE), four lab-fabricated TFCs (M-2.0, M-1.0, M-0.5, M-0.2), and the support of lab-fabricated TFCs (LX). The membranes were immersed in a series of Na_2SO_4 solutions (0.1, 0.25, 0.5, 0.75, 1.0, and 1.5 M) during the measurements. Measurements were performed at ambient temperature (22 °C), and the error bars represent standard deviation from triplicated membrane samples.

its potential viability as an affordable supporting electrolyte for various electrochemical flow systems, including those for alkaline sorbent regeneration in DAC. We expect similar resistance trends to hold for any salt. For each type of membrane, R_m decreased as the electrolyte concentration increased, which is consistent with previous findings.[19,47] The two commercial PFSMs showed very similar resistance with less than a 5.4% difference between at each concentration. Consistent with the observation from Shi et al.,[19] the commercial RO and NF membranes exhibited the highest resistances among all the membranes, especially at low electrolyte concentrations. Compared to Nafion and FKE, the fabricated TFC series demonstrated similar resistances across all concentrations. For example, the resistances of Nafion and M-2.0 were 16.3 ± 2.0 and 17.2 ± 0.8 Ω cm^2 in

https://doi.org/10.1021/acsapm.4c00001
ACS Appl. Polym. Mater. 2024, 6, 2022−2030

0.25 M Na_2SO_4, respectively, and 7.5 ± 0.9 and 7.1 ± 1.1 Ω cm^2 in 1.0 M Na_2SO_4. Among the fabricated TFCs, the membrane resistance decreased as the monomer concentration decreased, i.e., $R_{M\text{-}2.0} > R_{M\text{-}1.0} > R_{M\text{-}0.5} > R_{M\text{-}0.2}$. This trend correlates with the PA layer thickness (Table 1), i.e., thinner membranes exhibited lower resistance. These resistance trends are generally consistent with measured voltages during the early stages of a 19.7 mA cm^{-2} electrolysis measurement (see Figure S4) in the configuration shown in Figure 1c. M-0.2 provides the lowest measured voltage, roughly 160 mV lower than Nafion after 5 min of electrolysis, and XLE provides the highest when they are used in the cell, suggesting lower transport losses from the lower resistance membranes. We also measured the resistance of the porous support without a PA layer (LX), and the results indicated that the porous support contributed to the majority of the overall resistance given the similarity between its resistance and that of all lab-fabricated PA-TFCs. The support is a PES ultrafiltration membrane with 300 kDa molecular weight cut off and 220 μm thickness. Compared to the extremely thin PA active layer, which is less than 70 nm in all membranes, the thick PES layer poses significant resistance that in most cases overwhelms the resistance of the PA active layer. This observation suggests that further support optimization could dramatically reduce the membrane resistance and thus decrease the overall cell potential during operation. Given the statistical similarity between the resistance of the LX membrane and all fabricated PA-TFCs, we cannot quantify the conductivity of the PA layer directly and hence only report membrane resistance here.

3.3. Membrane Charge Density. The charge densities of all the TFC membranes at different pH levels are shown in Figure 3. The charge density of PA-based membranes all

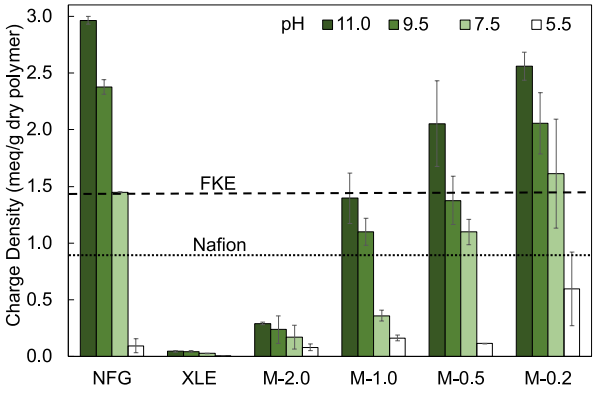

Figure 3. Charge density of PA layers isolated from various PA-TFC membranes measured with the QCM at different pH levels. The reported charge densities of FKE (dashed line) and Nafion (dotted line) were taken from manufacture specification sheets. The error bars represent standard deviation from duplicated membrane samples.

demonstrated strong dependency on solution pH with higher charge densities at higher pH levels, which is consistent with previous findings.[35,40,48] This can be explained by the fact that the negatively charged sites are a result of deprotonation of free carboxylic groups that are typically present after the interfacial polymerization, and the degree of deprotonation is a function of pH. Among all of the membranes, XLE showed the lowest charge density. As the only RO membrane, XLE has the tightest cross-linking structure, which presumably greatly reduces the total free carboxylic groups per unit mass PA. Similarly, among lab-fabricated membranes, the degree of polymerization likely decreased as the PIP monomer content decreased relative to the TMC content, resulting in more carboxylic group end terminations that lead to a higher charge density.[49] The same trend holds at all pH levels. In comparison, the charge density of commercial CEMs is not sensitive to pH given the very low pK_a (∼−7) of the sulfonate groups contained in them. We note in passing that our initial attempts to incorporate sulfonate groups into the PA structure using an appropriately functionalized amine monomer (taurine) were unsuccessful; the poor reactivity of taurine with TMC resulted in no sulfonate incorporation. Further attempts to incorporate strongly acidic functional groups could enable PA-based CEMs in acidic media. Nevertheless, compared to Nafion, most loose PA membranes (NFG, M-1.0, M-0.5, M-0.2) showed a higher charge density at pH values higher than 7.5. This is an encouraging result which indicates that in applications with alkaline solutions, PA-based membranes have the capacity to function as CEMs.

3.4. Solute Permeation Measurement. The permeation coefficients of NaCl and Na_2SO_4 of different membranes are shown in Figure 4. In general, for any membrane, the permeation coefficient of NaCl (1.32×10^{-8}–8.77×10^{-7} m/s) is about one magnitude higher than that of Na_2SO_4 (1.80×10^{-9}–1.63×10^{-8} m/s). This result can be explained by a stronger Donnan exclusion effect for divalent negative ions, such as SO_4^{2-}. This is also consistent with salt rejection trends in pressure-driven dead-end flow filtration experiments (Figure S2 in Section S3, Supporting Information). All membranes exhibited low Na_2SO_4 permeation, with the fabricated membranes showing the slowest Na_2SO_4 transport. We attribute this result to the high charge density of the fabricated membranes. The NFG membrane, which has the high charge density but relatively fast salt transport, was an exception most likely due to some imperfection of the NFG membrane surface, which could promote additional salt (and water) permeation. In terms of NaCl permeation, Nafion and FKE showed the slowest permeation, followed by XLE, M-2.0, and then the NF and lab-prepared membranes with thinner PA layers. In the case of only monovalent ions present in the solution, the thickness of the membrane also appeared to play an important role in governing salt permeation in addition to Donnan exclusion. As shown in Figure 4, XLE and M-2.0 demonstrated much lower permeation as they have relatively tight structure, while NaCl permeation increased as the PA thickness decreased for M-1.0, M-0.5, and M-0.2.

3.5. Ion Transference Number Measurement. The results in Figure 5a show the Na^+ transference number, t_+, in the system of 0.5 M Na_2SO_4 (catholyte) and 1 M NaCl (anolyte). In this configuration, the measurement provides an estimate of the transference number expected in a membrane in contact with a 0.5 M Na_2SO_4 solution given that Na^+ and SO_4^{2-} are expected to predominantly carry current in this configuration. Both commercial CEMs demonstrated the highest Na^+ selectivity with a t_+ value of about 1, indicating essentially no SO_4^{2-} transport across the membrane. Importantly, all of the fabricated TFCs had very high Na^+ transference numbers, approaching those of the commercial CEMs. M-2.0 had the highest t_+ of 0.99 ± 0.01, with t_+ slightly decreasing as the membrane monomer concentration decreases. The commercial RO showed comparable t_+ of 0.97 ± 0.01, while the commercial NF has a lower t_+ of 0.93 ± 0.00. The support membrane without the PA layer (LX)

https://doi.org/10.1021/acsapm.4c00001
ACS Appl. Polym. Mater. 2024, 6, 2022−2030

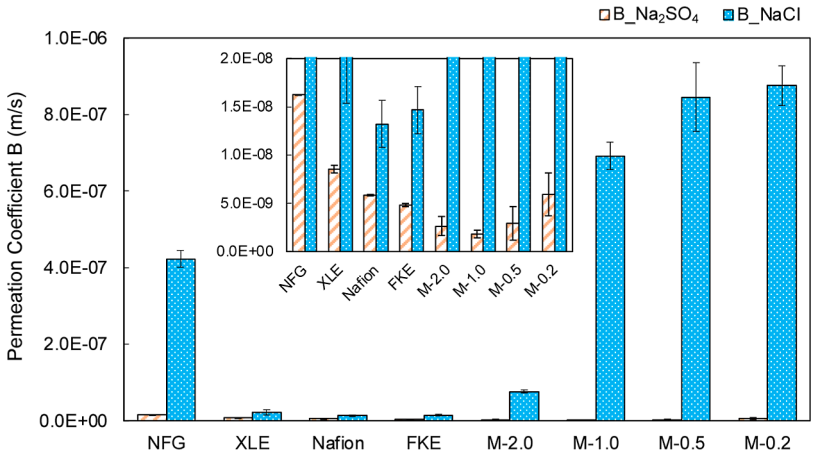

Figure 4. Permeation coefficient of NaCl and Na_2SO_4 measured with 1 M solutions. The inset is the same plot shown on a different scale to visualize the Na_2SO_4 coefficients. The error bars represent standard deviation from triplicated membrane samples.

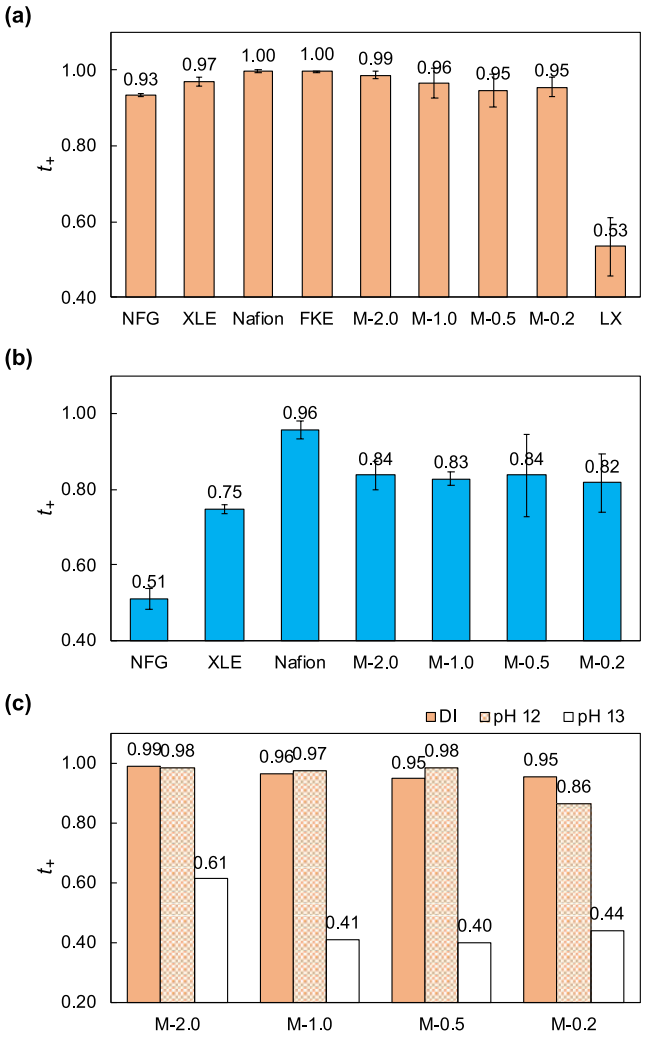

Figure 5. Transference number measurement results. (a) Estimated Na^+ transference number in 0.5 M Na_2SO_4 (catholyte) of fresh membranes. (b) Estimated Na^+ transference number in 1 M NaCl (anolyte) with fresh membrane. (c) Estimated Na^+ transference number in 0.5 M Na_2SO_4 (catholyte) with the membrane soaked for 60 days in different solutions (DI water, 0.01 M NaOH at pH 12, and 0.1 M NaOH at pH 13). The error bars represent standard deviation from triplicate membrane samples.

showed a t_+ of 0.53 ± 0.08; however, it is worth noting that unlike in the PA layers, the pore size of the support membrane (molecular weight cutoff of 300 kDa, which is on the order of 0.1 μm) is much larger than the hydrodynamic radius of any ions in the studied systems, such that this value is an estimate of the transference number of a 0.5 M Na_2SO_4 solution rather than the LX membrane itself. This value is slightly higher than a previously measured t_+ for a 0.5 M Na_2SO_4 solution (0.38),[50] likely a result of the non-negligible diffusion of Cl^- from the anolyte to catholyte chamber through the membrane. Nevertheless, this confirms that the close-to-unity t_+ values in PA-TFCs are attributed to the selective PA layer.

When using 1 M KCl (catholyte) and 1 M NaCl (anolyte) as electrolytes, which enables estimation of the expected transference number for a membrane in contact with a 1 M NaCl solution (Figure 5b), Nafion exhibited the highest t_+ among all of the membranes. Regardless of the difference in fabrication recipe, all fabricated TFCs exhibited a t_+ above 0.8 (within experimental error), indicating reasonable selectivity toward Na^+ transport over Cl^-. The commercial PA-TFCs showed much lower t_+ values compared to other membranes. For each type of membrane, the t_+ value is higher in the SO_4^{2-} electrolyte compared to the Cl^- electrolyte, which can be explained by the size and charge of the species. While SO_4^{2-} is larger than Cl^-, which tends to make SO_4^{2-} migration through the membrane slower than that of Cl^-, all the membranes are negatively charged, meaning that more highly charged anions experience stronger repulsion from the membrane due to stronger Donnan exclusion.[51] As a result, the membranes are more effective at impeding SO_4^{2-} transport than Cl^-. The sum of the transport numbers for all ions in solution always equals unity and specifically in our system

$$t_+ + t_- + t_{H^+} + t_{OH^-} = 1 \quad (8)$$

As both t_{H^+} and t_{OH^-} are negligible in all the experiments given their very low concentrations (always <0.01 M) compared to the concentrations of Na^+ and its counteranion, eq 8 simplifies to

$$t_+ + t_- = 1 \quad (9)$$

To confirm that pH does not significantly impact these measurements, we also measured the Na^+ transference numbers of all membranes in 0.1 M buffered bicarbonate solutions (pH 6−7) and observed similarly high Na^+

https://doi.org/10.1021/acsapm.4c00001
ACS Appl. Polym. Mater. 2024, 6, 2022−2030

transference numbers (Section S4 in Supporting Information). For each kind of PA-TFC tested, $t_{SO_4^{2-}}$ is smaller than t_{Cl^-}, and thus t_+ is always higher in electrolyte containing multivalent anions.

Since the amide bonds in PA-based membranes are susceptible to hydrolysis under alkaline conditions,[52,53] we tested the membrane stability in "near" strong alkaline environments. The fabricated TFCs were soaked for 60 days in DI water (pH = 6.3), 0.01 M NaOH (pH = 12), 0.1 M NaOH (pH = 13), and 1 M NaOH (pH = 14). Fresh soaking solutions were changed every 5 days and stored at 4 °C at all times to limit the biofilm growth on the membranes. We measured Na^+ transference of these membranes with 0.5 M Na_2SO_4 (catholyte) and 1 M NaCl (anolyte), and the results are shown in Figure 5c. All of the TFCs soaked in DI after 60 days still demonstrated similar t_+ compared to fresh membranes. Most membrane transference numbers were maintained at pH 12 except for a slight decrease in t_+ for M-0.2. This could be explained by the thinner PA layer of the M-0.2 membrane compared to that of other membranes, making it more susceptible to small amounts of degradation. There was a significant decrease in t_+ ranging from 38 to 54% for membranes soaked in pH 13 solutions, indicating severe membrane degradation under this condition. As expected, the TFC membranes experienced even more degradation after being soaked in pH 14 solutions as the membrane texture became visually softer and thinner (t_+ data not shown in figure). The stability of PA-based membrane operating in alkaline conditions over the long term requires further research and improvement. Some research efforts have shown promise on developing alkali-resistant PA membranes,[52,54−58] which could address the stability challenge and promote the application of PA-based membranes in electrochemical flow systems.

4. CONCLUSIONS

This work evaluated the possibility of using re-engineered PA-based composite membranes as CEMs in electrochemical applications. Thinner TFC membrane PA layers with a higher bulk charge density can be prepared by using lower amine concentrations in a typical interfacial polymerization solution. By comparing a series of fabricated TFC membranes, two commercial TFC membranes (XLE and NFG), and two types of commercial CEMs (Nafion 117 and FKE), we found that the best performing PA membranes demonstrate comparable performance compared to traditional PFSMs, with both the membrane resistance and Na^+ transference number being similar, particularly when multivalent anions are present. The TFC porous support membrane was found to predominantly account for the prepared TFC membrane resistance, suggesting that further optimization of its structure could greatly improve the ion transport across the membrane. With the PES support tested in this study, we found that all fabricated TFC membranes exhibited Na_2SO_4 Na^+ transference numbers greater than 0.95 and NaCl Na^+ transference numbers around 0.85. Further enhancements to ion selectivity could be envisioned through modification of the polymerization conditions or incorporation of monomers that contain either strongly acidic or basic constituents (e.g., sulfonate groups or ammonium groups) or functional groups that specifically interact with targeted ions. Overall, there remain challenges for using PA membranes compared to PFSMs in strongly alkaline electrolytes due to their relatively poor long-term stability; however, they may be suitable for "near-neutral" pH applications, such as electrodialysis and certain redox flow batteries. Furthermore, the low cost and scalability of PA-TFCs provide an incentive to further optimize their application in electrochemical flow systems.

■ ASSOCIATED CONTENT

Supporting Information

The Supporting Information is available free of charge at https://pubs.acs.org/doi/10.1021/acsapm.4c00001.

Polyamide TFC membrane fabrication procedure, representative Nyquist plots from membrane resistance measurements, membrane performance in pressure-driven tests, transference number measurements in buffered system, representative voltage profile from transference number measurements, representative concentration profile from transference number measurements, and polyamide active layer isolation procedure (PDF)

■ AUTHOR INFORMATION

Corresponding Author

Bryan D. McCloskey − *Energy Storage and Distributed Resources Division, Lawrence Berkeley National Laboratory, Berkeley, California 94720, United States; Department of Chemical and Biomolecular Engineering, University of California, Berkeley, California 94720, United States;* orcid.org/0000-0001-6599-2336; Email: bmcclosk@berkeley.edu

Authors

Jingbo Wang − *Energy Storage and Distributed Resources Division, Lawrence Berkeley National Laboratory, Berkeley, California 94720, United States;* orcid.org/0000-0003-1911-123X

Jeonghoon Lim − *Energy Storage and Distributed Resources Division, Lawrence Berkeley National Laboratory, Berkeley, California 94720, United States;* orcid.org/0000-0002-5254-2296

Monong Wang − *Department of Civil and Environmental Engineering, University of California, Berkeley, California 94720, United States*

Baoxia Mi − *Department of Civil and Environmental Engineering, University of California, Berkeley, California 94720, United States;* orcid.org/0000-0003-3185-1820

Daniel J. Miller − *Chemical Sciences Division, Lawrence Berkeley National Laboratory, Berkeley, California 94720, United States;* orcid.org/0000-0003-4245-3270

Complete contact information is available at: https://pubs.acs.org/10.1021/acsapm.4c00001

Notes

The authors declare no competing financial interest.

■ ACKNOWLEDGMENTS

The authors would like to thank Dr. Wenbo Yang for his assistance with ICP-OES analysis. This work was funded by Berkeley Lab Laboratory Directed Research & Development (LDRD) Program. Any opinions, findings, and conclusions or recommendations expressed in this material are those of the

authors and do not necessarily reflect the views of the Department of Energy.

■ ABBREVIATIONS

CEM, cation exchange membrane; CsCl, cesium chloride; DAC, direct air CO_2 capture; EIS, electrochemical impedance spectroscopy; ICP-OES, inductively coupled plasma with an optical emission system; NF, nanofiltration; PA, polyamide; PFSM, perfluorinated sulfonated membranes; PIP, piperazine; QCM, quartz crystal microbalance; RO, reverse osmosis; TFC, thin-film composite; TMC, trimesoyl chloride

■ REFERENCES

(1) Asawa, T. Material Properties of Cation Exchange Membranes for Chloralkali Electrolysis, Water Electrolysis and Fuel Cells. *J. Appl. Electrochem.* **1989**, *19* (4), 566−570.
(2) Yee, R. S. L.; Rozendal, R. A.; Zhang, K.; Ladewig, B. P. Cost Effective Cation Exchange Membranes: A Review. *Chem. Eng. Res. Des.* **2012**, *90* (7), 950−959.
(3) Ran, J.; Wu, L.; He, Y.; Yang, Z.; Wang, Y.; Jiang, C.; Ge, L.; Bakangura, E.; Xu, T. Ion Exchange Membranes: New Developments and Applications. *J. Membr. Sci.* **2017**, *522*, 267−291.
(4) Li, X.; Zhang, H.; Mai, Z.; Zhang, H.; Vankelecom, I. Ion Exchange Membranes for Vanadium Redox Flow Battery (VRB) Applications. *Energy Environ. Sci.* **2011**, *4* (4), 1147.
(5) Kitto, D.; Kamcev, J. The Need for Ion-Exchange Membranes with High Charge Densities. *J. Membr. Sci.* **2023**, *677*, 121608.
(6) FilmTec Reverse Osmosis Membranes Technical Manual Water Solutions, 2023. https://www.dupont.com/content/dam/dupont/amer/us/en/water-solutions/public/documents/en/RO-NF-FilmTec-Manual-45-D01504-en.pdf (accessed 2023-06-06).
(7) Biesheuvel, P. M.; Porada, S.; Elimelech, M.; Dykstra, J. E. Tutorial Review of Reverse Osmosis and Electrodialysis. *J. Membr. Sci.* **2022**, *647*, 120221.
(8) Chaudhury, S. G. The Donnan Membrane Equilibrium. *Nature* **1943**, *152* (3846), 76−77.
(9) Yaroshchuk, A. E. Dielectric Exclusion of Ions from Membranes. *Adv. Colloid Interface Sci.* **2000**, *85* (2−3), 193−230.
(10) Freger, V. Dielectric Exclusion, an Eminence Grise. *Adv. Colloid Interface Sci.* **2023**, *319*, 102972.
(11) Kezia, K.; Lee, J.; Ogieglo, W.; Hill, A.; Benes, N. E.; Kentish, S. E. The Transport of Hydronium and Hydroxide Ions through Reverse Osmosis Membranes. *J. Membr. Sci.* **2014**, *459*, 197−206.
(12) Cheng, W.; Lu, X.; Yang, Y.; Jiang, J.; Ma, J. Influence of Composition and Concentration of Saline Water on Cation Exchange Behavior in Forward Osmosis Desalination. *Water Res.* **2018**, *137*, 9−17.
(13) Ma, G.; Xu, X.; Tesfai, M.; Zhang, Y.; Wang, H.; Xu, P. Nanocomposite Cation-Exchange Membranes for Wastewater Electrodialysis: Organic Fouling, Desalination Performance, and Toxicity Testing. *Sep. Purif. Technol.* **2021**, *275*, 119217.
(14) Pusch, W. Comparison of Transport of Alkali Halides and Nitrates across Asymmetric Cellulose Acetate and Polyamide, Composite Poly(Etherurea), and Cation Exchange Membranes. *Desalination* **1991**, *83* (1−3), 261−270.
(15) Huang, T.-C.; Yeh, T.-C.; Huang, H.-Y.; Ji, W.-F.; Lin, T.-C.; Chen, C.-A.; Yang, T.-I.; Yeh, J.-M. Electrochemical Investigations of the Anticorrosive and Electrochromic Properties of Electroactive Polyamide. *Electrochim. Acta* **2012**, *63*, 185−191.
(16) Shaffer, D. L.; Feldman, K. E.; Chan, E. P.; Stafford, G. R.; Stafford, C. M. Characterizing Salt Permeability in Polyamide Desalination Membranes Using Electrochemical Impedance Spectroscopy. *J. Membr. Sci.* **2019**, *583*, 248−257.
(17) Zhao, C.; Zhang, Y.; Jia, Y.; Li, B.; Tang, W.; Shang, C.; Mo, R.; Li, P.; Liu, S.; Zhang, S. Polyamide Membranes with Nanoscale Ordered Structures for Fast Permeation and Highly Selective Ion-Ion Separation. *Nat. Commun.* **2023**, *14* (1), 1112.
(18) Epsztein, R.; DuChanois, R. M.; Ritt, C. L.; Noy, A.; Elimelech, M. Towards Single-Species Selectivity of Membranes with Sub-nanometre Pores. *Nat. Nanotechnol.* **2020**, *15* (6), 426−436.
(19) Shi, L.; Rossi, R.; Son, M.; Hall, D. M.; Hickner, M. A.; Gorski, C. A.; Logan, B. E. Using Reverse Osmosis Membranes to Control Ion Transport during Water Electrolysis. *Energy Environ. Sci.* **2020**, *13*, 3138−3148.
(20) Sheng, F.; Hou, L.; Wang, X.; Irfan, M.; Shehzad, M. A.; Wu, B.; Ren, X.; Ge, L.; Xu, T. Electro-Nanofiltration Membranes with Positively Charged Polyamide Layer for Cations Separation. *J. Membr. Sci.* **2020**, *594*, 117453.
(21) Nativ, P.; Fridman-Bishop, N.; Gendel, Y. Ion Transport and Selectivity in Thin Film Composite Membranes in Pressure-Driven and Electrochemical Processes. *J. Membr. Sci.* **2019**, *584*, 46−55.
(22) Dai, Q.; Liu, Z.; Huang, L.; Wang, C.; Zhao, Y.; Fu, Q.; Zheng, A.; Zhang, H.; Li, X. Thin-Film Composite Membrane Breaking the Trade-off between Conductivity and Selectivity for a Flow Battery. *Nat. Commun.* **2020**, *11* (1), 13.
(23) Bason, S.; Oren, Y.; Freger, V. Ion Transport in the Polyamide Layer of RO Membranes: Composite Membranes and Free-Standing Films. *J. Membr. Sci.* **2011**, *367* (1−2), 119−126.
(24) Wang, X.; Tan, M.; Wang, M.; Zhou, G.; Liu, F.; Zhang, Y. Porphyrin Thin-Film Composite Cation Exchange Membranes Enable High Retention of Amino Acids in Electrodialysis. *Sep. Purif. Technol.* **2021**, *279*, 119729.
(25) Wang, W.; Liu, R.; Tan, M.; Sun, H.; Niu, Q. J.; Xu, T.; Nikonenko, V.; Zhang, Y. Evaluation of the Ideal Selectivity and the Performance of Selectrodialysis by Using TFC Ion Exchange Membranes. *J. Membr. Sci.* **2019**, *582*, 236−245.
(26) Hou, L.; Wu, B.; Yu, D.; Wang, S.; Shehzad, M. A.; Fu, R.; Liu, Z.; Li, Q.; He, Y.; Afsar, N. U.; Jiang, C.; Ge, L.; Xu, T. Asymmetric Porous Monovalent Cation Perm-Selective Membranes with an Ultrathin Polyamide Selective Layer for Cations Separation. *J. Membr. Sci.* **2018**, *557*, 49−57.
(27) Bason, S.; Oren, Y.; Freger, V. Characterization of Ion Transport in Thin Films Using Electrochemical Impedance Spectroscopy II: Examination of the Polyamide Layer of RO Membranes. *J. Membr. Sci.* **2007**, *302* (1−2), 10−19.
(28) Freger, V.; Bason, S. Characterization of Ion Transport in Thin Films Using Electrochemical Impedance Spectroscopy. I. Principles and Theory. *J. Membr. Sci.* **2007**, *302* (1−2), 1−9.
(29) Lee, W.; Permatasari, A.; Kwon, Y. Neutral PH Aqueous Redox Flow Batteries Using an Anthraquinone-Ferrocyanide Redox Couple. *J. Mater. Chem. C* **2020**, *8* (17), 5727−5731.
(30) Beh, E. S.; De Porcellinis, D.; Gracia, R. L.; Xia, K. T.; Gordon, R. G.; Aziz, M. J. A Neutral PH Aqueous Organic-Organometallic Redox Flow Battery with Extremely High Capacity Retention. *ACS Energy Lett.* **2017**, *2* (3), 639−644.
(31) Shu, Q.; Legrand, L.; Kuntke, P.; Tedesco, M.; Hamelers, H. V. M. Electrochemical Regeneration of Spent Alkaline Absorbent from Direct Air Capture. *Environ. Sci. Technol.* **2020**, *54* (14), 8990−8998.
(32) Xie, W.; Geise, G. M.; Freeman, B. D.; Lee, H.-S.; Byun, G.; McGrath, J. E. Polyamide Interfacial Composite Membranes Prepared from M-Phenylene Diamine, Trimesoyl Chloride and a New Disulfonated Diamine. *J. Membr. Sci.* **2012**, *403−404*, 152−161.
(33) Ghosh, A. K.; Jeong, B.-H.; Huang, X.; Hoek, E. M. V. Impacts of Reaction and Curing Conditions on Polyamide Composite Reverse Osmosis Membrane Properties. *J. Membr. Sci.* **2008**, *311* (1−2), 34−45.
(34) Atkinson, A. J. A. J.; Wang, J.; Grzebyk, K.; Zhang, Z.; Jung, D.; Zeng, D.; Pollard, A.; Gold, A.; Coronell, O. Scalable Fabrication of Anti-Biofouling Membranes through 2-Aminoimidazole Incorporation during Polyamide Casting. *J. Membr. Sci.* **2019**, *579*, 151−161.
(35) Perry, L. A.; Coronell, O. Reliable, Bench-Top Measurements of Charge Density in the Active Layers of Thin-Film Composite and Nanocomposite Membranes Using Quartz Crystal Microbalance Technology. *J. Membr. Sci.* **2013**, *429*, 23−33.
(36) Lin, L.; Feng, C.; Lopez, R.; Coronell, O. Identifying Facile and Accurate Methods to Measure the Thickness of the Active Layers of

https://doi.org/10.1021/acsapm.4c00001
ACS Appl. Polym. Mater. 2024, 6, 2022−2030

Thin-Film Composite Membranes - a Comparison of Seven Characterization Techniques. *J. Membr. Sci.* **2016**, *498*, 167−179.
(37) Shackelford, J. F. *Introduction to Materials Science for Engineers*, 8th ed.; Pearson College Div, 2014.
(38) Kamcev, J.; Sujanani, R.; Jang, E. S.; Yan, N.; Moe, N.; Paul, D. R.; Freeman, B. D. Salt Concentration Dependence of Ionic Conductivity in Ion Exchange Membranes. *J. Membr. Sci.* **2018**, *547*, 123−133.
(39) Wang, J.; Kingsbury, R. S.; Perry, L. A.; Coronell, O. Partitioning of Alkali Metal Salts and Boric Acid from Aqueous Phase into the Polyamide Active Layers of Reverse Osmosis Membranes. *Environ. Sci. Technol.* **2017**, *51* (4), 2295−2303.
(40) Wang, J.; Armstrong, M. D.; Grzebyk, K.; Vickers, R.; Coronell, O. Effect of Feed Water PH on the Partitioning of Alkali Metal Salts from Aqueous Phase into the Polyamide Active Layers of Reverse Osmosis Membranes. *Environ. Sci. Technol.* **2021**, *55* (5), 3250−3259.
(41) Heyrovská, R. Ionic Concentrations and Hydration Numbers of "Supporting Electrolytes. *Electroanalysis* **2006**, *18* (4), 351−361.
(42) Kingsbury, R. S.; Zhu, S.; Flotron, S.; Coronell, O. Microstructure Determines Water and Salt Permeation in Commercial Ion Exchange Membranes. *ACS Appl. Mater. Interfaces* **2018**, *10* (46), 39745−39756.
(43) Geise, G. M.; Freeman, B. D.; Paul, D. R. Sodium Chloride Diffusion in Sulfonated Polymers for Membrane Applications. *J. Membr. Sci.* **2013**, *427*, 186−196.
(44) Yasuda, H.; Lamaze, C.; Ikenberry, L. D. Permeability of Solutes through Hydrated Polymer Membranes. Part I. Diffusion of Sodium Chloride. *Makromol. Chem.* **1968**, *118* (1), 19−35.
(45) Vardner, J. T.; Russell, S. T.; Brady, N. W.; Inaba, Y.; Kumar, S. K.; West, A. C. Application of Concentrated Solution Theory to the Measurement of Salt Transference Numbers in Ion-Selective Membranes. *J. Electrochem. Soc.* **2020**, *167* (2), 020546.
(46) Russell, S. T.; Pereira, R.; Vardner, J. T.; Jones, G. N.; Dimarco, C.; West, A. C.; Kumar, S. K. Hydration Effects on the Permselectivity-Conductivity Trade-Off in Polymer Electrolytes. *Macromolecules* **2020**, *53* (3), 1014−1023.
(47) Zhu, S.; Kingsbury, R. S.; Call, D. F.; Coronell, O. Impact of Solution Composition on the Resistance of Ion Exchange Membranes. *J. Membr. Sci.* **2018**, *554*, 39−47.
(48) Coronell, O.; Mariñas, B. J.; Zhang, X.; Cahill, D. G. Quantification of Functional Groups and Modeling of Their Ionization Behavior in the Active Layer of FT30 Reverse Osmosis Membrane. *Environ. Sci. Technol.* **2008**, *42* (14), 5260−5266.
(49) Petersen, R. J. Composite Reverse Osmosis and Nanofiltration Membranes. *J. Membr. Sci.* **1993**, *83*, 81.
(50) Braun, B. M.; Weingartner, H. Transference Numbers of Aqueous NaCl and Na2SO4 at 25C from EMF Measurements with Sodium-Selective Glass Electrodes. *J. Solution Chem.* **1985**, *14* (9), 675−686.
(51) Helfferich, F. *Ion Exchange*; McGraw-Hill: New York, 1962.
(52) Dalwani, M.; Benes, N. E.; Bargeman, G.; Stamatialis, D.; Wessling, M. Effect of PH on the Performance of Polyamide/Polyacrylonitrile Based Thin Film Composite Membranes. *J. Membr. Sci.* **2011**, *372* (1−2), 228−238.
(53) Yao, C. W.; Burford, R. P.; Fane, A. G.; Fell, C. J. D.; McDonogh, R. M. Hydrolysis and Other Phenomena Affecting Structure and Performance of Polyamide 6 Membrane. *J. Appl. Polym. Sci.* **1987**, *34* (7), 2399−2408.
(54) Schlesinger, R.; Götzinger, G.; Sixta, H.; Friedl, A.; Harasek, M. Evaluation of Alkali Resistant Nanofiltration Membranes for the Separation of Hemicellulose from Concentrated Alkaline Process Liquors. *Desalination* **2006**, *192* (1−3), 303−314.
(55) Song, N.; Shan, W.; Xie, X.; Sun, Q.; Yu, L.; Dong, L. Design and Construct Alkali-Responsive Nanocontainers for Self-Healing Thin-Film Composite Reverse Osmosis Membranes. *Desalination* **2022**, *535*, 115823.
(56) Xie, Q.; Zhang, S.; Xiao, Z.; Hu, X.; Hong, Z.; Yi, R.; Shao, W.; Wang, Q. Preparation and Characterization of Novel Alkali-Resistant Nanofiltration Membranes with Enhanced Permeation and Antifouling Properties: The Effects of Functionalized Graphene Nanosheets. *RSC Adv.* **2017**, *7* (30), 18755−18764.
(57) Li, L.-Q.; Liu, X.-H.; Tang, Y.-J.; Xu, Z.-L. How Does Alkali Etching Work on the Polyamide Membrane to Obtain an *m*-Phenylenediamine-Based NF Membrane? *Ind. Eng. Chem. Res.* **2022**, *61* (16), 5536−5546.
(58) Lee, K. P.; Zheng, J.; Bargeman, G.; Kemperman, A. J. B.; Benes, N. E. PH Stable Thin Film Composite Polyamine Nanofiltration Membranes by Interfacial Polymerisation. *J. Membr. Sci.* **2015**, *478*, 75−84.

https://doi.org/10.1021/acsapm.4c00001
ACS Appl. Polym. Mater. 2024, 6, 2022−2030